[1.] **Sefiu A. ONITILO, Deborah O. DANIEL**

# HEAT AND MASS TRANSFER EFFECTS ON MAGNETOHYDRODYNAMIC OSCILLATORY FLOW OF A NON-NEWTONIAN FLUID IN AN ASYMMETRIC WAVY CHANNEL

[1.] Department of Mathematical Sciences, Olabisi Onabanjo University, Ago-Iwoye, NIGERIA

**Abstract:** This paper examined the magnetohydrodynamic (MHD) oscillatory flow of non-Newtonian fluids within an asymmetric wavy channel, focusing on the impacts of heat and mass transfer effects, particularly under optically thin conditions with radiation. Through rigorous MATLAB simulations, the study dissects how varying parameters such as the Peclet number, radiation parameter, and Schmidt number intricately influence the fluid's velocity, temperature, and concentration profiles. Notably, the findings underscore the critical role of phase angle adjustments, especially at $\varphi = \pi/2$, in modulating flow characteristics, thereby shedding light on the complex interdependencies between magnetic fields, chemical reactions, and viscoelastic parameters in shaping non-Newtonian fluid dynamics. This contribution is pivotal for enhancing the understanding and optimization of industrial processes involving MHD flows of non-Newtonian fluids.

**Keywords:** Heat and Mass Transfer, Magnetohydrodynamic (MHD), Oscillatory Flow Dynamics, Optically Thin Radiation, Non-Newtonian Fluids

## 1. INTRODUCTION

The study of heat and mass transfer within non-Newtonian fluids under the influence of magnetohydrodynamic (MHD) conditions, particularly within asymmetric wavy channels, represents a compelling confluence of fluid dynamics, thermodynamics, and magnetism. Non-Newtonian fluids, distinguished by their shear rate-dependent viscosity, exhibit behaviours markedly distinct from their Newtonian counterparts, particularly under MHD influences. These behaviours are not merely academic curiosities but are of paramount importance due to the broad spectrum of applications, from industrial processes to the cutting edge of biomedical engineering.

The intrigue surrounding non-Newtonian fluids in MHD contexts is well-founded, given their ubiquity and critical roles in various sectors. For instance, the unique flow properties of blood in magnetic fields hold significant promise for revolutionary medical diagnostics and treatments, as highlighted in [18]. In the industrial domain, fluids with non-Newtonian characteristics are frequently processed under conditions where magnetic fields and complex channel geometries are the norms, as discussed in [19]. The introduction of heat and mass transfer into this equation introduces additional layers of complexity and practical relevance, particularly when considering the impact of asymmetric wavy channels. These channels, with their non-uniform wall geometry, significantly influence flow patterns and the rates of heat and mass transfer, as the channel's waviness induces secondary flows that can enhance mixing, thereby potentially improving heat transfer efficiency but also complicating the prediction and management of these flows.

The application of a magnetic field to fluid flow within such channels can modify pressure drops, alter heat transfer characteristics, and influence flow stability, with research indicating that MHD effects can vary significantly due to the intricate interplay between fluid rheology and magnetic forces ([4]). The study of oscillatory MHD flows, in particular, has been identified for its potential to augment mixing and heat transfer across a range of applications, from microfluidics to bioengineering processes ([7, 15. 11, 12]). Several studies have ventured into the effects of heat and mass transfer on the magnetohydrodynamic oscillatory flow of non-Newtonian fluids in asymmetric wavy channels, investigating a plethora of parameters such as Reynolds number, volume fraction, Hartmann number, amplitude of wavelength, and non-uniform heat flux. The foundational work of [13, 14] on oscillatory flow of couple stress fluids and the effects of suction and injection in porous media, alongside [9]'s considerations of ferrofluid flows under non-uniform magnetic fields in wavy channels, underscore the delicate balance between magnetic field application and heat transfer enhancement. Further, [5]'s insights into peristaltic pumping in curved channels, and the analyses in [2] and [17] on heat and mass transfer effects in MHD flows, especially in configurations involving porous media and nanofluids, extend


ISSN 1584 – 2665 (printed version); ISSN 2601 – 2332 (online); ISSN-L 1584 – 2665

our comprehension of these complex systems. Notably, [1] and [8] have elucidated the impact of microchannel wave amplitude on heat transfer and the effects of non-uniform heating within wavy channels, respectively.

The intricate dynamics of these systems often necessitate advanced computational fluid dynamics (CFD) techniques for analysis, given the challenges in resolving the complexity of flow and heat transfer in non-Newtonian fluids under MHD conditions within asymmetric wavy channels through analytical methods alone. The peristaltic flow of a Johnson-Segalman fluid in an asymmetric curved channel has also been studied, considering the presence of heat and mass transfer. The results have shown the physical features of flow variables and geometric parameters through graphs and stream functions [6].The investigation into the dynamics of Casson fluid flow within an uneven channel takes into account the influences of magnetohydrodynamics, the presence of a porous medium, thermal radiation, the effect of viscous dissipation, and chemical reactions. This comprehensive study reveals that the velocity and concentration distributions of the fluid demonstrate contrasting behaviors when compared between the channel's upper and lower boundaries ({5]). The work of [3], focusing on the impacts of magnetic fields and radiation on unsteady free convective MHD flow, alongside [20]'s investigation into time-averaged transport in oscillatory squeeze flow of viscoelastic fluids, exemplifies the significant influence of magnetic fields and radiation on flow characteristics. Similarly, [16] and [10] have contributed to our understanding of thermal radiation, Hall current effects, and the enhancements in heat transfer efficiency due to fluid elasticity and oscillatory forcing.

By delving into the underlying mechanisms that govern fluid flow, heat, and mass transfer in such intricate configurations, this paper aims to further the advancement of fluid mechanics and its applications in engineering and industrial processes, potentially leading to more efficient designs in medical devices and diagnostic equipment, and fostering reduced energy consumption and environmental impact.

## 2. MATHEMATICAL FORMULATION

Consider an unsteady, viscous, incompressible, electrically conductive, and chemically reactive fluid. This fluid traverses through an asymmetric, sinuously shaped channel imbued with a porous medium. The entire system is subjected to a uniform magnetic field and engages in radiative heat transfer, including a heat source. The channel's boundaries are defined by: channel walls are given by:

$$\begin{aligned} H_1 &= \bar{d}_1 + \bar{a}_1 \cos\frac{2\pi x}{\lambda} \\ H_2 &= -\bar{d}_2 - \bar{b}_1 \cos\left(\frac{x\pi x}{\lambda} + \varphi\right) \end{aligned} \tag{1}$$

where $\bar{a}_1, \bar{b}_1, \bar{d}_1, \bar{d}_2$ and $\varphi$ satisfy the condition of $\bar{a}_1^2 + \bar{b}_1^2 + 2\bar{a}_1\bar{b}_1\cos\varphi \le (\bar{d}_1 + \bar{d}_2)^2$ ([15]) as shown in Figure 1.

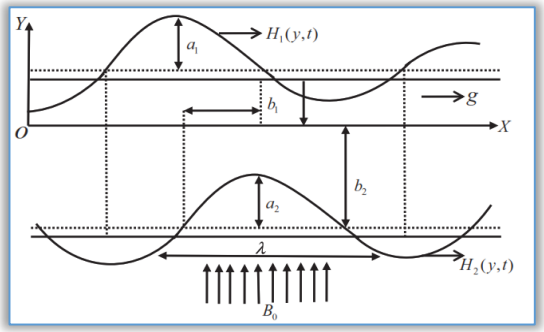


Figure 1: Physical model of the problem

It is assumed that the electromagnetic force generated by the field, which is characterized by low electrical conductivity, is minimal. A Cartesian coordinate system, denoted as $(\bar{x}, \bar{y})$, is introduced with the $\bar{x}$-axis aligned with the channel's center and the $\bar{y}$-axis representing the perpendicular distance. Within the context of Boussinesq's approximation for incompressible fluids, the mathematical equations that describe the flow field under these conditions are:

Momentum Equation:

$$\frac{\partial \bar{u}}{\partial \bar{t}} = -\frac{1}{\rho}\frac{\partial \bar{P}}{\partial \bar{x}} + \nu\frac{\partial^2 \bar{u}}{\partial \bar{y}^2} - \frac{\nu}{k}\bar{u} - \frac{\sigma\mu_e^2 H^2}{\rho}\bar{u} + g\beta_T(\bar{T} - \bar{T}_2) + g\beta_C(\bar{C} - \bar{C}_2) + K_0\frac{\partial^3 u}{\partial y^2\,\partial t} \tag{2}$$

Energy Equation:

$$\frac{\partial \bar{T}}{\partial \bar{t}} = \frac{k}{\rho C_p}\frac{\partial^2 \bar{T}}{\partial \bar{y}^2} - \frac{1}{\rho C_p}\frac{\partial q_r}{\partial y} + \frac{Q_0}{\rho C_p}(\bar{T} - \bar{T}_2) \tag{3}$$

Species Equation:

$$\frac{\partial \bar{C}}{\partial \bar{t}} = D\frac{\partial^2 \bar{C}}{\partial \bar{y}^2} - \bar{K}_r(\bar{C} - \bar{C}_2) \tag{4}$$

The boundary conditions for the velocity, temperature and concentration fields are:


ISSN 1584 – 2665 (printed version); ISSN 2601 – 2332 (online); ISSN-L 1584 – 2665

$$\begin{aligned} \bar{u} = 0, \overline{T} = \overline{T}_1, \overline{C} = \overline{C}_1 \quad \text{on} \quad \bar{y} = H_1 \\ \bar{u} = 0, \overline{T} = \overline{T}_2, C = \overline{C}_2 \quad \text{on} \quad \bar{y} = H_2 \end{aligned} \tag{5}$$

where $\bar{u}$ represents the fluid's velocity in the direction along the plate, denoted as the $x$-direction. The symbol $\bar{t}$ stands for time, while $\bar{p}$ indicates the pressure within the system. The gravitational force is represented by $g$, and $\bar{q}_r$ denotes the radiative heat flux. The terms $\beta_T$ and $\beta_C$ refer to the coefficients of volumetric expansion due to changes in temperature and concentration, respectively. $C_p$ is the specific heat at constant pressure. $T_1$ and $T_2$ are the temperatures of the fluid far from and close to the wall, respectively. $T$ signifies the fluid's temperature, and $C$ represents the concentration of a species within the fluid. The density of the fluid is given by $\rho$, and its electrical conductivity is denoted by $\sigma$. Thermal conductivity is represented by $K$, while $\overline{K}$ stands for the permeability coefficient of the porous medium. The magnetic permeability is indicated by $\mu_e$, with $H$ representing the magnetic field intensity. The fluid's conductivity is given by $\sigma_e$, and its density is again denoted by $\rho$. The coefficient of kinematic viscosity is represented by $v$. Additionally, $K_0$ is the viscoelastic parameter, and $Q_0$ refers to the heat source or sink within the system. The assumption here is that the wall temperatures, represented as $\overline{T}_0$ and $\overline{T}_w$, are elevated to a degree that enables the transfer of heat through radiation.

Under an optically thin fluid, the expression for the radiative flux term is described as:

$$\frac{\partial q_r}{\partial y} = 4(\overline{T} - \overline{T}_2)I \tag{6}$$

where

$$I = \int_0^\infty K_{\lambda w} \frac{\partial e_{b\lambda}}{\partial T} d\lambda \tag{7}$$

$K_{\lambda w}$ denotes the absorption coefficient at the wall, $e_{b\lambda}$ represents the Planck function, and $I$ signifies the absorption coefficient.

Consequently, by integrating equation (6) into equation (3), the resulting formulation is obtained as

$$\frac{\partial \overline{T}}{\partial \bar{t}} = \frac{k}{\rho C_p}\frac{\partial^2 \overline{T}}{\partial \bar{y}^2} + 4I(\overline{T} - \overline{T}_2) + \frac{Q_0}{\rho C_p}\overline{T} \tag{8}$$

To express equations (2)-(4) along its associated boundary conditions in a non-dimensionless form, the study incorporates several non-dimensional parameters:

$$x = \frac{\bar{x}}{a}, y = \frac{\bar{y}}{a^2}, \quad u = \frac{\bar{u}}{U}, \quad t = \frac{\bar{t}U}{a}, \quad Ra = \frac{16\sigma \overline{T}_w^{\,3}}{3\rho C_p U a}, \quad K = \frac{\bar{k}}{a^2},$$

$$Re = \frac{Ua}{v}, \quad Q = \frac{kQ_0}{\rho C_p U^2}, \quad R = \frac{4kvI}{\rho C_p U^2}$$

$$\theta = \frac{\overline{T} - \overline{T}_0}{\overline{T}_w - \overline{T}_0}, \quad \phi = \frac{\overline{C} - \overline{C}_0}{\overline{C}_w - \overline{C}_0}, \quad Sc = \frac{v}{D}, \quad P = \frac{a\overline{P}}{\rho v U}, \quad kr = \frac{\bar{k} r a}{U},$$

$$M = \frac{a^2 \rho_e \sigma \mu_e^2 H_0^2}{\rho v}, \quad k_0 = K_0 \frac{U^2}{va}$$

$$Pe = \frac{\rho U a C_p}{k}, \quad G_r = \frac{g\beta(\overline{T}_w - \overline{T}_0)a^2}{vU}, \quad G_c = \frac{g\beta(\overline{C}_w - \overline{C}_0)a^2}{vU}, \quad h_1 = \frac{H_1}{\bar{a}_1}, \quad h_2 = \frac{H_2}{\bar{a}_2}$$

The dimensionalise equations for the governing equation under optically thin limit radiation is

$$Re\frac{\partial u}{\partial t} = -\frac{\partial P}{\partial x} + \frac{\partial^2 u}{\partial y^2} - \left(\frac{1}{K} + M\right)u + G_r\theta + G_c\phi + k_0\frac{\partial^3 u}{\partial y^2 \partial t} \tag{9}$$

$$Pe\frac{\partial \theta}{\partial t} = \frac{\partial^2 \theta}{\partial y^2} + (R + Q)\theta \tag{10}$$

$$\frac{\partial \phi}{\partial t} = \frac{1}{ScRe}\frac{\partial^2 \phi}{\partial y^2} - k_r\phi \tag{11}$$

Accordingly, the boundary conditions, when expressed in a dimensionless form, are articulated as follows:

$$\begin{aligned} u = 0, \quad \theta = 1, \quad \phi = 1, \quad \text{on} \quad y = h_1 \\ u = 0, \quad \theta = 0, \quad \phi = 0, \quad \text{on} \quad y = h_2 \end{aligned} \tag{12}$$

where

$$\begin{aligned} h_2 &= d + a\cos 2\pi x \\ h_2 &= -d - b\cos(2\pi x + \varphi) \end{aligned} \tag{13}$$

$a, b, d$ and $\varphi$ satisfy the condition of $a^2 + b^2 + 2ab\cos\varphi \le (1 + d)^2$

Here, $Gr$, $H$, $J$, $Pe$, $Re$, $Da$, and $S = (1/Da)$ denote, respectively, the Grashof number, Hartmann number, Radiation parameter, Peclet number, Reynolds number, Darcy number, and a parameter representing the shape factor of the porous medium.


ISSN 1584 – 2665 (printed version); ISSN 2601 – 2332 (online); ISSN-L 1584 – 2665

## 3. METHOD OF SOLUTION

To derive solutions for pure oscillatory flow, we start with a proposed solution, aiming to address the mathematical equations spanning from (9)-(12).

$$\begin{cases} -\frac{\partial P}{\partial x} = \lambda e^{iwt}, \\ u(y,t) = u_0(y)e^{iwt}, \\ \theta(y,t) = \theta_0(y)e^{iwt}, \\ \phi(y,t) = \phi_0 e^{iwt} \end{cases} \tag{14}$$

where $-\lambda$ represents the constant amplitude of oscillation for the pressure gradient, while $\omega$ denotes the oscillation frequency. Substituting the values for equation (14) into (9)-(12). follow by rearranging and multiplying by $e^{-iwt}$, we obtain

$$\frac{d^2\theta_0}{dy^2} + n_1^2\theta_0 = 0 \tag{15}$$

where $n_1^2 = (Q + R - iwPe)$

$$\frac{d^2\theta_0}{dy^2} + n_2^2\theta_0 = 0 \tag{16}$$

where $n_2^2 = \frac{iwPe}{1+Ra}$

$$\frac{d^2\phi_0}{dy^2} - l^2\phi_0 = 0 \tag{17}$$

where $l^2 = (kr + iw)ScRe$

The corresponding boundary conditions becomes:

$$\begin{aligned} u_0 = 0, \quad \theta_0 = 1, \quad \phi_0 = 1, \qquad & \text{on} \quad y = h_1 \\ u_0 = 0, \quad \theta_0 = 0, \quad \phi_0 = 0, \qquad & \text{on} \quad y = h_2 \end{aligned} \tag{18}$$

Solving equation (17) result in

$$\phi(y,t) = \phi_0(y)e^{iwt} = \frac{\sinh l(h_2 - y)}{\sinh l(h_2 - h_1)} e^{iwt} \tag{19}$$

$$\theta(y,t) = \theta_0(y)e^{iwt} = \frac{\sin n(h_2 - y)}{\sin n(h_2 - h_1)} e^{iwt} \tag{20}$$

$$\begin{aligned} u(y,t) &= u_0(y)e^{iwt} \\ &= \left\{\left(\frac{\beta_2}{(n^2+m^2)} - \frac{\beta_3}{(l^2-m^2)} + \frac{\beta_1}{m^2}\right)\frac{\sinh m(h_2 - y)}{\sinh m(h_2 - h_1)} + \frac{\beta_2}{(n^2+m^2)}\frac{\sin n(h_2 - y)}{\sin n(h_2 - h_1)}\right. \\ &\left. - \frac{\beta_3}{(l^2-m^2)}\frac{\sinh l(h_2 - y)}{\sinh l(h_2 - h_1)} + \frac{\beta_1}{m^2}\right\} e^{iwt} \end{aligned} \tag{21}$$

In the study of boundary layer flow, the Nusselt number, Sherwood number, and skin-friction coefficient stand out as critical physical measures. These parameters facilitate understanding the temperature distribution across the flow, enabling the calculation of the heat transfer rate at the channel's boundaries.

This rate, when expressed through the Nusselt number, offers a quantifiable measure of the thermal exchange efficiency between the fluid and its surrounding surfaces, is given by:

$$\begin{aligned} Nu &= -\left(\frac{\partial\theta}{\partial y}\right)_{y=h_1,h_2} \\ &= \frac{n\cos n(h_2 - y)}{\sin n(h_2 - h_1)} e^{iwt} \end{aligned} \tag{22}$$

Upon determining the concentration field, it becomes possible to ascertain the mass transfer coefficient rate at the channel's walls. This is quantifiable through the Sherwood number, as follows:

$$\begin{aligned} Sh &= -\left(\frac{\partial\phi}{\partial y}\right)_{y=h_1,h_2} \\ &= \frac{l\cosh l(h_2 - y)}{\sinh n(h_2 - h_1)} e^{iwt} \end{aligned} \tag{23}$$

Upon determining the velocity field, it is possible to ascertain the skin friction along the channel walls. This is represented in a dimensionless form as follows:

$$\begin{aligned} \tau &= -\mu\left(\frac{\partial u}{\partial y}\right)_{y=h_1,h_2} \\ &= -\mu\left\{\left(-\frac{\beta_2}{(n^2+m^2)} - \frac{\beta_3}{(l^2-m^2)} + \frac{\beta_1}{m^2}\right)\frac{m\cosh m(h_2 - y)}{\sinh m(h_2 - h_1)} - \frac{\beta_2}{(n^2+m^2)}\frac{n\cos n(h_2 - y)}{\sin n(h_2 - h_1)}\right. \\ &\left. + \frac{\beta_3}{(l^2-m^2)}\frac{l\cosh l(h_2 - y)}{\sinh l(h_2 - h_1)}\right\} e^{iwt} \end{aligned} \tag{24}$$


ISSN 1584 – 2665 (printed version); ISSN 2601 – 2332 (online); ISSN-L 1584 – 2665

## 4. NUMERICAL SOLUTION

This section delves into how various factors pertinent to the research affect velocity, temperature, and concentration profiles, in addition to impacting skin friction, Nusselt, and Sherwood numbers, particularly under conditions of optically thin limit radiation. The effects are visually depicted through figures and a table for clear understanding and analysis. For the sake of analysis the following values are used for calculations

$$\mathrm{M} = 2.0, \mathrm{R} = 2.0, \mathrm{Q} = 3.0, \mathrm{Pe} = 0.71, \mathrm{Gc} = 10.0, \mathrm{Gr} = 10.0, \mathrm{Kr} = 0.01, \mathrm{K} = 1.0, \mathrm{Sc} = 0.6.$$

From the temperature profile and velocity profile under optically thin limit radiation for phase angle $\varphi = \pi/2$, it is observed that there is a downward movement from $\mathrm{y} = -2$ to $\mathrm{y} = -0.6$ and alternate at $\mathrm{y} = -0.6$, then an upward movement is noticed from $\mathrm{y} = -0.6$ to $\mathrm{y} = 0.8$. Furthermore, the motion of the fluid, when initiated by oscillatory actions, exhibits a peak velocity at the channel's midpoint, a phenomenon noticeable at a phase angle of $\varphi = 0$.When the phase angle is set to $\varphi = \frac{\pi}{2}$, leading to fluid movement driven by oscillations, the viscoelastic fluid demonstrates a periodic variation in its motion due to the asymmetry of the surface. This condition results in the amplitude of the response reaching its peak values at $\mathrm{y} = 0$ and $\mathrm{y} = -1.3$. Furthermore, it is found that both the velocity and temperature at $\varphi = \pi/2$ significantly exceed those observed when $\varphi = 0$. This phenomenon can be attributed to the augmentation of the phase angle, which plays a crucial role in altering these physical properties.

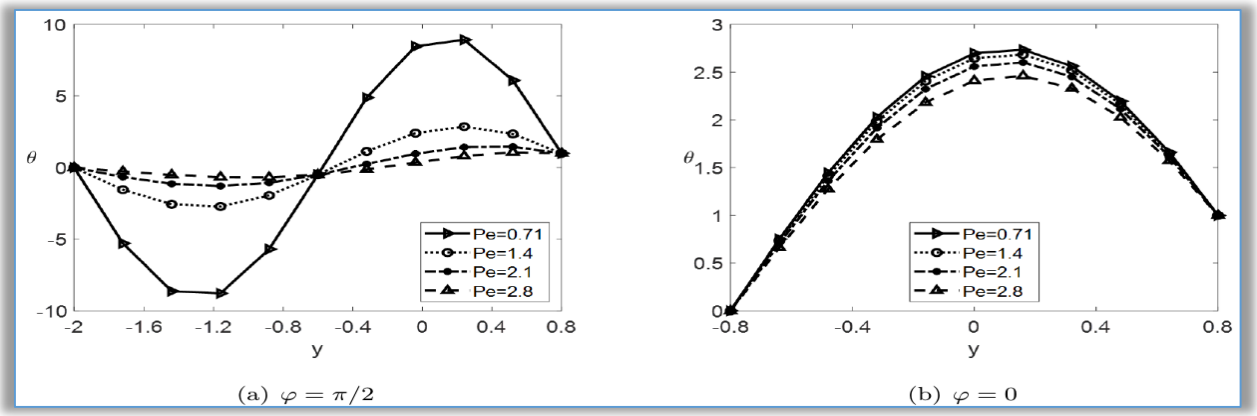


Figure 2: Temperature Profile at varied $\mathrm{Pe}$

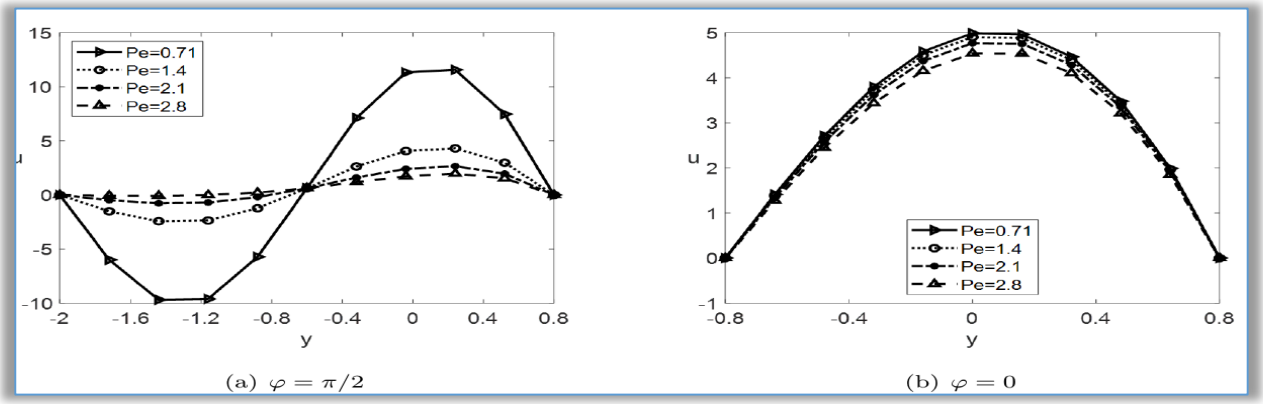


Figure 3: Velocity Profile at varied $\mathrm{Pe}$

Figures 2(a)-2(b) alongside Figures 3(a)-3(b) distinctly illustrate the distributions of velocity and temperature under optically thin radiation conditions, corresponding to various Peclet numbers $\mathrm{Pe}$ at phase angles $\varphi = 0$ and $\varphi = \pi/2$, respectively. An observable trend is the decrease in temperature with an escalation in $\mathrm{Pe}$. A similar trend is evident in the fluid's velocity profile; as $\mathrm{Pe}$ increases, the fluid's velocity diminishes for both $\varphi = 0$ and $\varphi = \pi/2$. From a physical standpoint, an elevation in the Peclet number signifies a distribution dominated by advection, whereas a lower value suggests a diffusive flow. Consequently, across the boundary layer for $\varphi = 0$ and $\varphi = \pi/2$, a diffuse flow of the fluid is observed. This is attributed to the fact that lower $\mathrm{Pe}$ values equate to an increased thermal conductivity of the fluid, facilitating a more rapid diffusion of heat away from the heated surface at higher $\mathrm{Pe}$ values. Thus,


ISSN 1584 – 2665 (printed version); ISSN 2601 – 2332 (online); ISSN-L 1584 – 2665

at lower Peclet numbers, the thermal boundary layer is more substantial, diminishing the rate of heat transfer.

Figures 4(a)-4(b) elucidate the impact of the viscoelastic parameter $\mathbf{k_0}$ on the velocity distribution under optically thin radiation conditions for $\varphi = 0$ and $\varphi = \pi/2$, respectively. It is noted that an increase in $\mathbf{k_0}$ values leads to a reduction in the fluid's velocity.

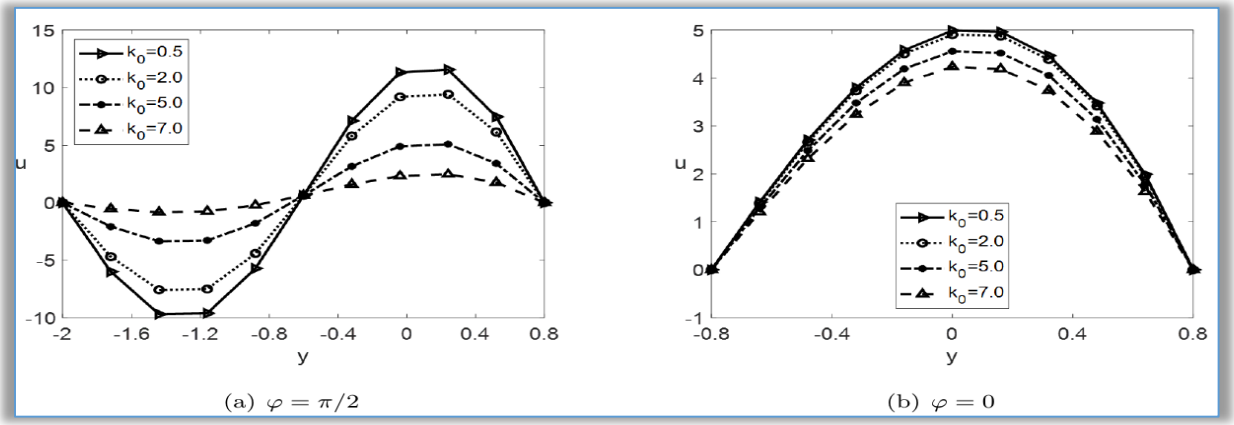


Figure 4: Velocity Profile at varied $\mathbf{k_0}$

Similarly, Figures 5(a)-5(b) expound on how the permeability parameter $\mathbf{K}$ influences the velocity profile under optically thin radiation conditions for phase angles $\varphi = 0$ and $\varphi = \pi/2$, respectively. It has been discerned that the velocity augments with $\mathbf{K}$. This is because an increase in $\mathbf{K}$ corresponds to a higher degree of porosity within the porous medium, thereby permitting a more unimpeded flow of the viscoelastic fluid through the channel. These findings align with documented literature and are corroborated by experimental evidence.

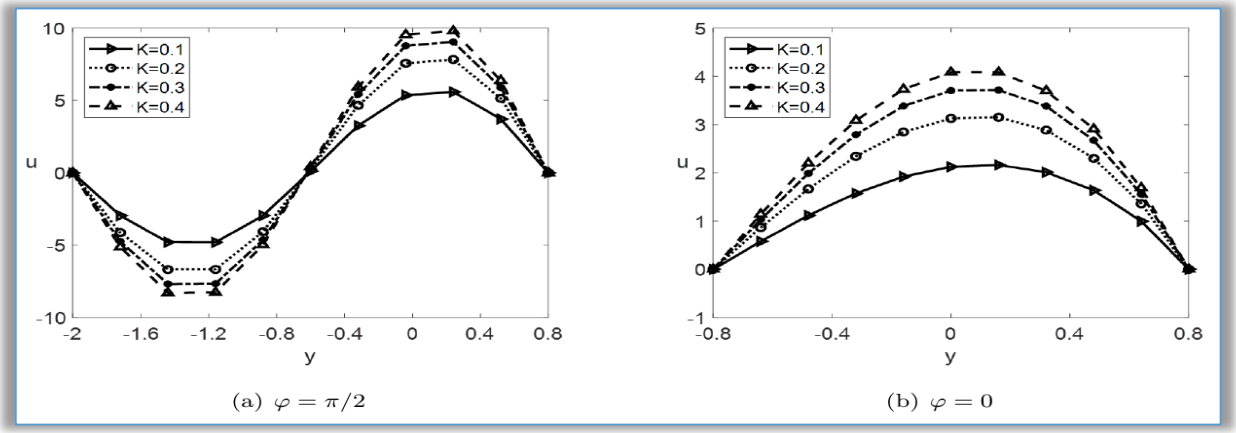


Figure 5: Velocity Profile at varied $\mathbf{K}$

Moreover, Figures 6(a)-6(b) and Figures 7(a)-7(b) display the velocity and concentration profiles under optically thin limit radiation at $\varphi = 0$ and $\varphi = \pi/2$ for diverse values of the chemical reaction parameter $\mathbf{Kr}$, respectively. A decline in both velocity and concentration profiles is observed when $\mathbf{Kr}$ increases, underscoring the significance of buoyancy effects induced by variations in concentration and temperature within the channel. Furthermore, a chemical reaction is seen to decelerate fluid velocity, indicating that a destructive reaction ($\mathbf{Kr} > 0$) diminishes the concentration field, thereby attenuating buoyancy effects engendered by concentration gradients and subsequently slowing the flow field. Additionally, the velocity is comparatively lower for $\varphi = 0$ than for $\varphi = \pi/2$, an observation that closely mirrors physical realities.

Figures 8(a)-8(b) and Figures 9(a) to 9(b) respectively depict the concentration and velocity distributions under optically thin limit radiation for varying Schmidt numbers $\mathbf{Sc}$ at phase angles $\varphi = 0$ and $\varphi = \pi/2$. An increase in $\mathbf{Sc}$ values is seen to elevate concentration distributions across the boundary layer for both considered phase angles. Additionally, an increase in the Schmidt number results in an elevated fluid velocity when $\varphi = 0$ and $\varphi = \pi/2$. Typically, a rise in the Schmidt number signifies a reduction in


ISSN 1584 – 2665 (printed version); ISSN 2601 – 2332 (online); ISSN-L 1584 – 2665

molecular diffusion, thereby enhancing the species concentration for smaller **Sc** values and reducing it for larger **Sc** values.

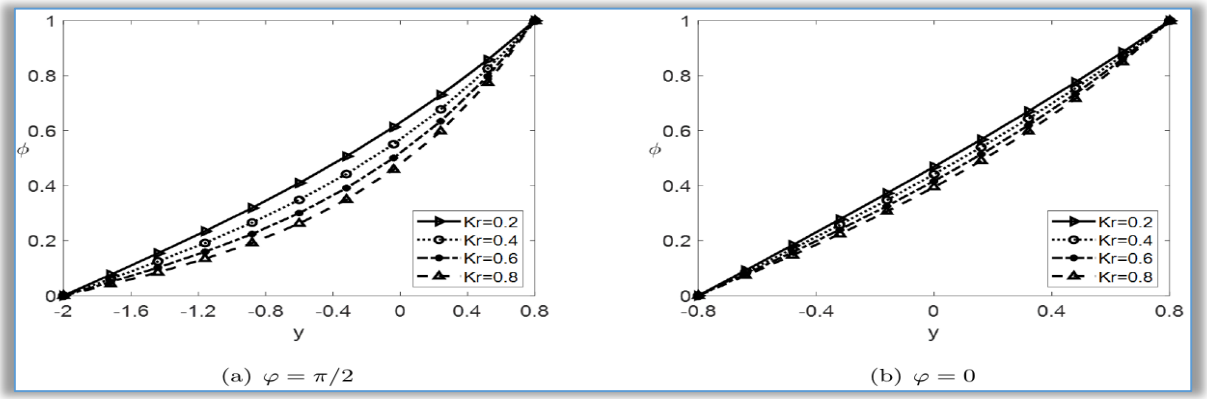


Figure 6: Concentration Profile at varied **Kr**

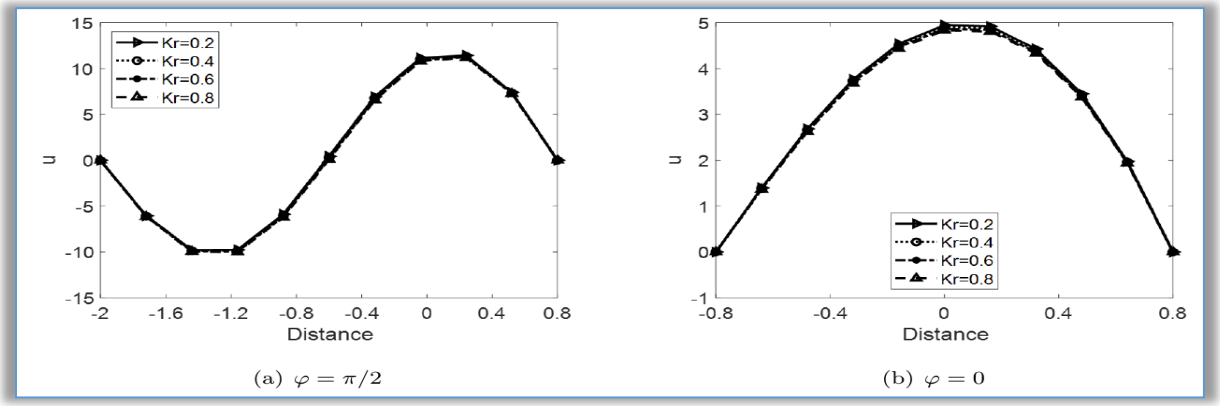


Figure 7: Velocity Profile at varied **Kr**

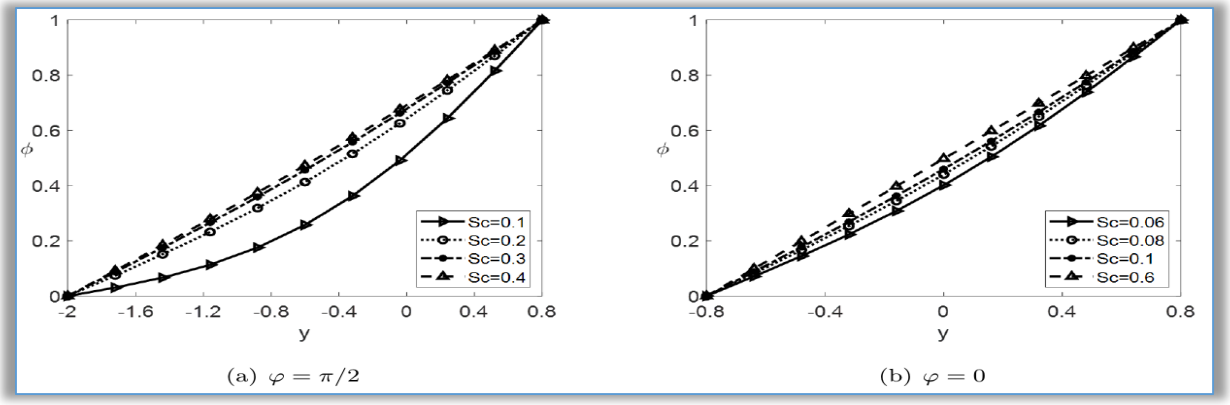


Figure 8: Concentration Profile at varied **Sc**

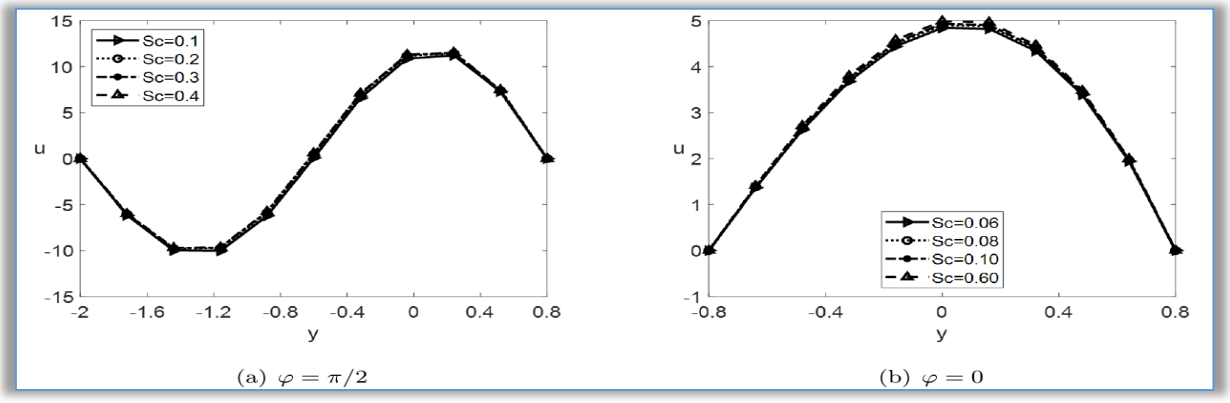


Figure 9: Velocity Profile at varied **Sc**


ISSN 1584 – 2665 (printed version); ISSN 2601 – 2332 (online); ISSN-L 1584 – 2665

Figures 10(a)-10(b) and Figures 11(a)-11(b) present the velocity and temperature profiles under optically thin limit radiation for varying heat generation parameters $\mathbf{Q}$ for $\boldsymbol{\varphi = 0}$ and $\boldsymbol{\varphi = \pi/2}$, respectively. An increase in $\mathbf{Q}$ results in heightened velocity and temperature distributions. The introduction of a thermal source implies thermal generation from the surface (owing to $\mathbf{T_w > T_\infty}$), thus increasing the temperature across the flow field. Consequently, as the parameter indicating the intensity of the heat source escalates, there is a notable and exponential increase in temperature emanating from the surface, a result that is well-supported from a physical standpoint.

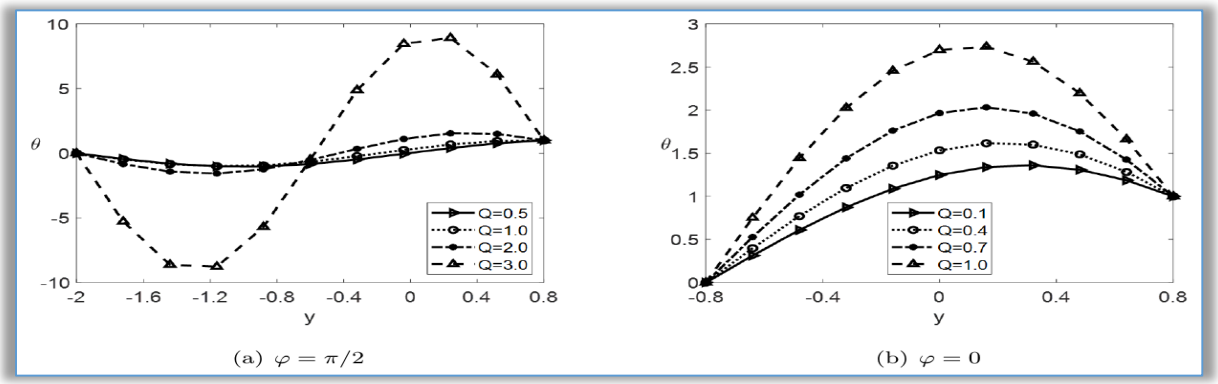


Figure 10: Temperature Profile at varied $\mathbf{Q}$

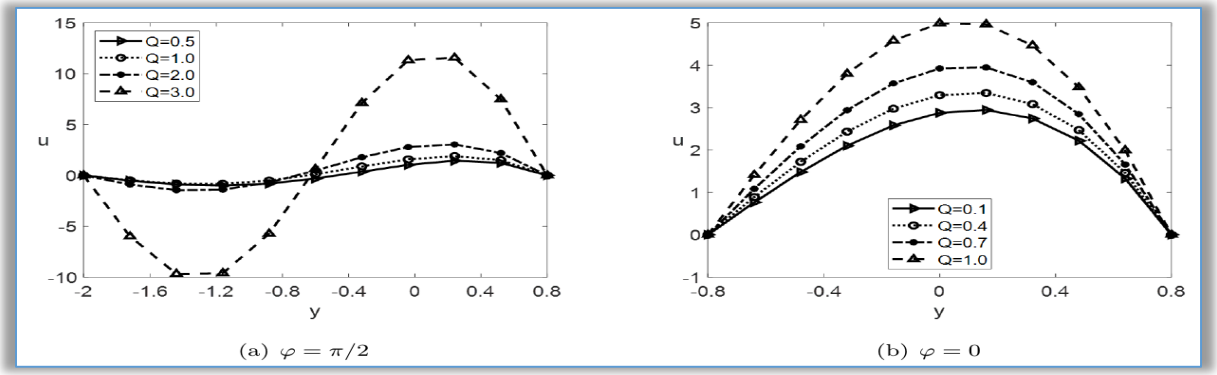


Figure 11: Velocity Profile at varied $\mathbf{Q}$

Figures 12(a)-12(b) illustrate the magnetic field parameter Mâ€™s effect on velocity distribution under optically thin radiation conditions for phase angles $\boldsymbol{\varphi = 0}$ and $\boldsymbol{\varphi = \pi/2}$. An increase in $\mathbf{M}$ down the surface is observed to reduce velocity, a phenomenon attributable to the Lorentz forceâ€"a resistive-type force emanating from the effect of a transverse magnetic field, likely decelerating the fluid's motion. This understanding is crucial for a range of industrial processes, especially in the realms of metal casting and the growth of semiconductor single crystals. These areas see a direct impact on product integrity from the dynamics of fluid flow and turbulence. The strategic application of magnetic fields has been identified as an effective method for controlling melt convection in systems undergoing solidification, enhancing the overall quality of the final product.

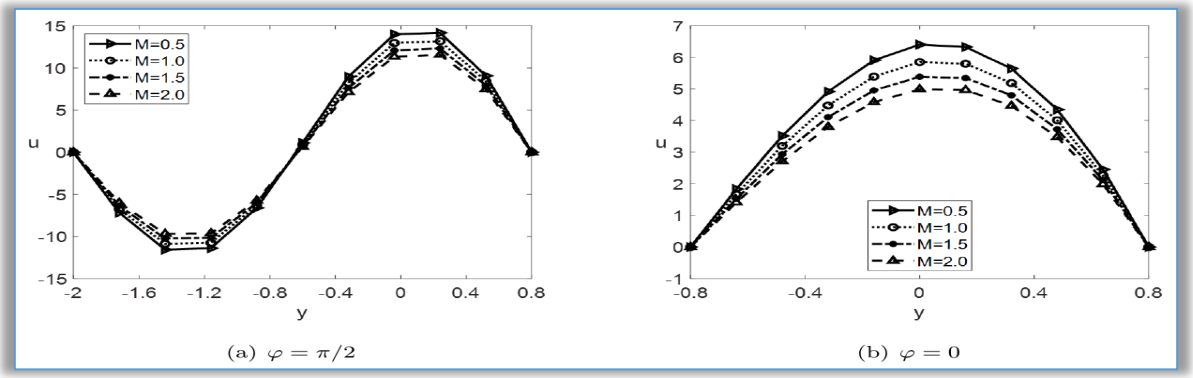


Figure 12: Velocity Profile at varied $\mathbf{M}$


ISSN 1584 – 2665 (printed version); ISSN 2601 – 2332 (online); ISSN-L 1584 – 2665

Figures 13(a)-13(b) and Figures 14(a)-14(b) respectively detail the velocity and temperature profiles under optically thin limit radiation for different thermal radiation parameters $\mathbf{R}$ at phase angles $\boldsymbol{\varphi = 0}$ and $\boldsymbol{\varphi = \pi/2}$. An increase in $\mathbf{R}$ is found to increase both the velocity and temperature of the viscoelastic fluid. An increase in thermal radiation heat production tends to disrupt the cohesive forces among the fluid's component particles more readily, thereby accelerating the fluid's velocity. Thus, reducing radiation emerges as a necessary strategy to expedite the cooling process.

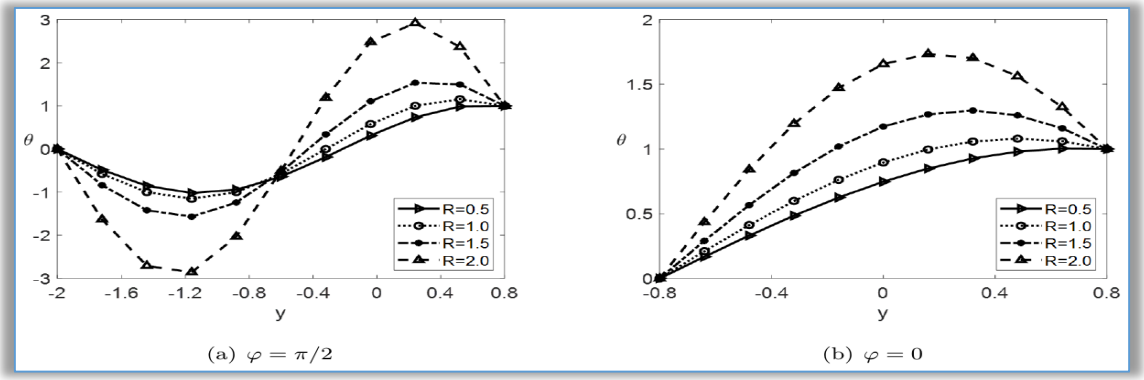


Figure 13: Temperature Profile at varied $\mathbf{R}$

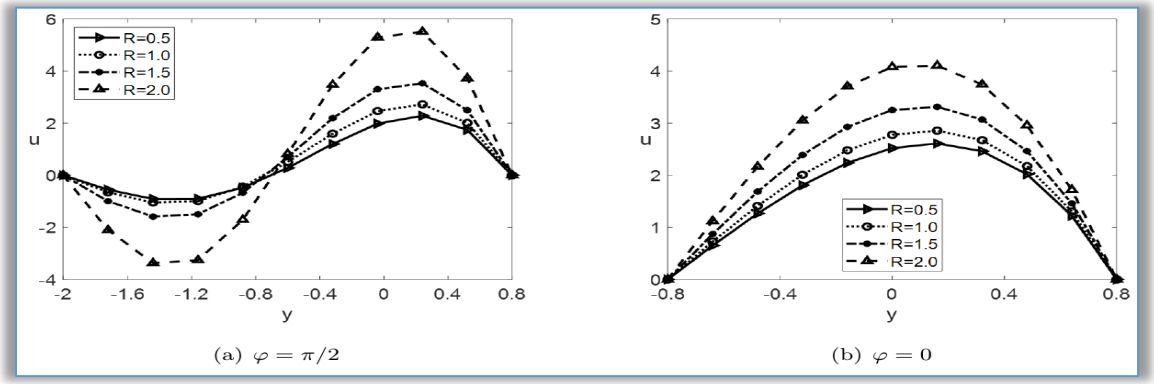


Figure 14: Velocity Profile at varied $\mathbf{R}$

Figures 15(a)-15(b) respectively illustrate the velocity distribution profiles under optically thin limit radiation for various Solutal Grashof Numbers $\mathbf{Gr}$ for $\boldsymbol{\varphi = 0}$ and $\boldsymbol{\varphi = \pi/2}$. An increase in $\mathbf{Gr}$ correlates with an increased velocity, both under optically thin and thick radiation limits, attributable to the buoyancy force acting on the fluid flow.

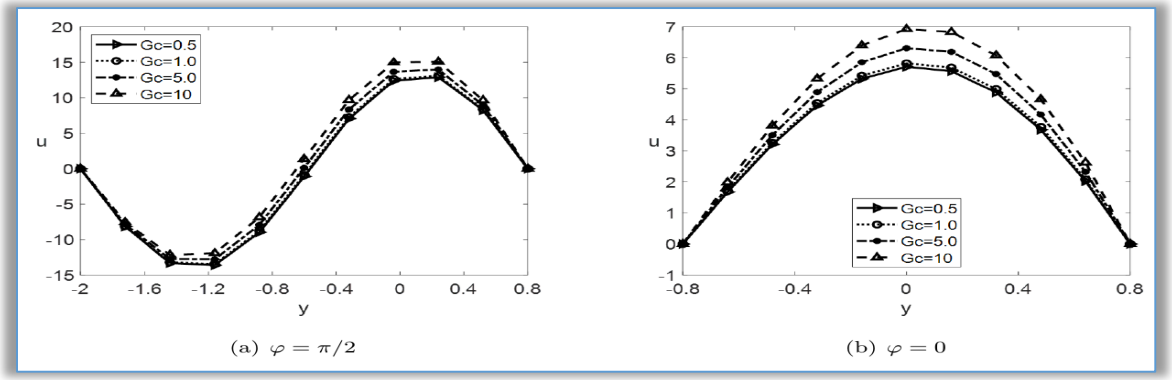


Figure 15: Velocity Profile at varied $\mathbf{Gc}$

Similarly, Figures 16(a)-16(b) respectively display the velocity distribution profiles under optically thin limit radiation for various values of the Modified Grashof Number $\mathbf{Gc}$ for $\boldsymbol{\varphi = 0}$ and $\boldsymbol{\varphi = \pi/2}$. An increase in $\mathbf{Gc}$ for $\boldsymbol{\varphi = 0}$ results in an increased fluid velocity. Moreover, for $\boldsymbol{\varphi = \pi/2}$, an increase in $\mathbf{Gc}$ towards the positive direction correlates with an increased fluid velocity, while a decrease towards the negative direction is observed. The influence of the buoyancy force on the fluid's movement can be attributed to this phenomenon.


ISSN 1584 – 2665 (printed version); ISSN 2601 – 2332 (online); ISSN-L 1584 – 2665

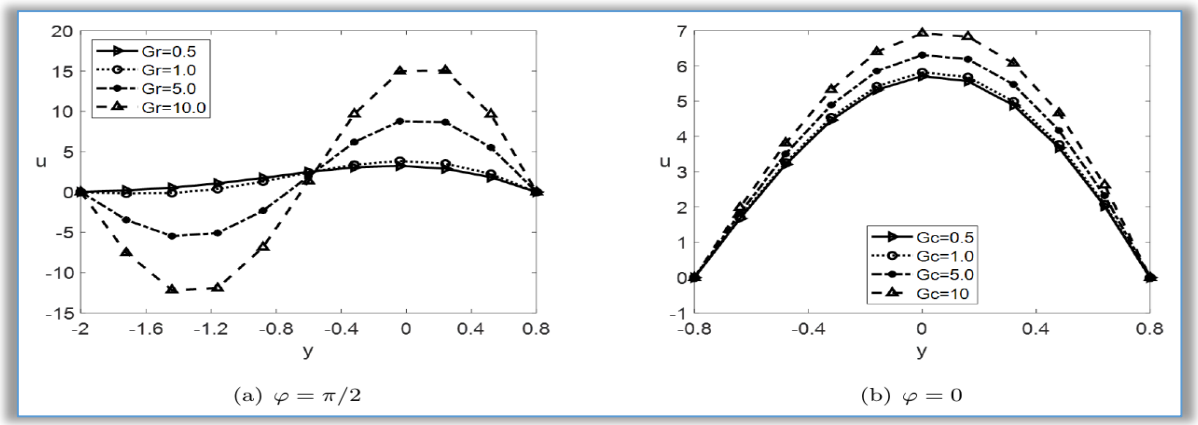


Figure 16: Velocity Profile at varied $\mathbf{Gr}$

## 5. CONCLUSION

This paper examines heat and mass transfer in magnetohydrodynamic (MHD) oscillatory flow of a non-Newtonian fluid within a porous medium channel, under optically thin limit radiation. Analytical solutions to the dimensionless governing equations, numerically evaluated using MATLAB, elucidate the impact of various parameters on velocity, temperature, and concentration profiles. Our analysis reveals distinct flow behavior changes with the phase angle, notably at $\boldsymbol{\varphi = \pi/2}$, where temperature and velocity significantly exceed those at $\boldsymbol{\varphi = 0}$. Key findings include a decrease in temperature and velocity with increased Peclet number ($\mathbf{Pe}$), whereas an increase in radiation parameter ($\mathbf{Ra}$) enhances both. Additionally, factors such as thermal Grashof number ($\mathbf{G_r}$), solutal Grashof number ($\mathbf{G_c}$), heat source parameter ($\mathbf{Q}$), and porous permeability ($\mathbf{K}$) positively influence fluid velocity, contrasting with the adverse effects of increased magnetic field, chemical reaction rate, and viscoelastic parameter. Concentration profiles improve with Schmidt number ($\mathbf{Sc}$) but decline with higher chemical reaction rates. This study highlights the intricate relationship between phase angle variations and flow characteristics, offering insights for optimizing relevant industrial applications.

**References**

[1] Anasuya, J. B., & Srinivas, S. (2023). Heat transfer characteristics of magnetohydrodynamic two fluid oscillatory flow in an inclined channel with saturated porous medium. Proceedings of the Institution of Mechanical Engineers, Part E: Journal of Process Mechanical Engineering

[2] Devi, M. P., & Srinivas, S. (2023). Heat transfer effects on the oscillatory MHD flow in a porous channel with two immiscible fluids. Nonlinear Analysis-Modelling and Control

[3] Ismail, M. N., Mohamadien, G. F., & Gaker, Ãœ. D. (2012). Finite difference solution of radiation on unsteady free convective magnetohydrodynamic flow past a vertical cylinder with heat and mass transfer. Retrieved from http://arxiv.org/abs/1206.3045v1

[4] Kumaran, V. (2019). Rheology of a suspension of conducting particles in a magnetic field. Journal of Fluid Mechanics, 871, 139-185

[5] Magesh, A., & Kothandapani, M. (2021). Heat and mass transfer analysis on non-Newtonian fluid motion driven by peristaltic pumping in an asymmetric curved channel. The European Physical Journal Special Topics

[6] Mehta, S. K., & Pati, S. (2021). Effect of Non-uniform Heating on Forced Convective Flow Through Asymmetric Wavy Channel. Lecture Notes in Mechanical Engineering.

[7] Misra, J., & Adhikary, S. (2016). MHD oscillatory channel flow, heat and mass transfer in a physiological fluid in presence of chemical reaction. Alexandria Engineering Journal, 55(1), 287â€"297

[8] Moslemi, M., Mahmoodnezhad, M., Edalatpanah, S. A., Zubair, S. A., & Khalifa, H. A. E. (2023). Magnetic Field Effect and Heat Transfer of Nanofluids within Waveform Microchannel. Cmes-computer Modeling in Engineering & Sciences

[9] Mousavi, S., Biglarian, M., Darzi, A. A. R., Farhadi, M., Afrouzi, H. H., & Toghraie, D. (2019). Heat transfer enhancement of ferrofluid flow within a wavy channel by applying a non-uniform magnetic field. Journal of Thermal Analysis and Calorimetry

[10] Nagrani, P. P., Municchi, F., Marconnet, A. M., & Christov, I. C. (2022). Two-fluid modeling of heat transfer in flows of dense suspensions. International Journal of Heat and Mass Transfer, 183(122068)

[11] Onitilo S. A. and Daniel D. O. (2020). The Effects of Heat and Mass Transfer on Magnetohydrodynamic Oscillatory Flow. Islamic University Multidisciplinary Journal IUMJ, 7 (2):332-341.

[12] Onitilo S. A., Daniel D. O. and Haruna H. A. (2020). Differential Transform Method for MHD Fluid Flow in a Porous Channel Under Optically Thick Limit Radiation. Anale. Seria InformaticÄƒ. . XVIII fasc. 2:135-140.

[13] Sasikumar, J., Bhati, D., & Bhaskar, V. (2020). Effect of heat and mass transfer on MHD oscillatory flow through asymmetric wavy channel in a porous medium with suction and injection. AIP Conference Proceedings

[14] Sasikumar, J., Gayathri, R., & Govindarajan, A. (2018). Heat and Mass Transfer Effects on MHD Oscillatory flow of a Couple Stress fluid in an Asymmetric Tapered channel. IOP Conference Series: Materials Science and Engineering

[15] Satya Narayana, P., Venkateswarlu, B., & Devika, B. (2016). Chemical reaction and heat source effects on MHD oscillatory flow in an irregular channel. Ain Shams Engineering Journal, 7(4), 1079-1088
[16] Shit, G. C., & Haldar, R. (2010). Combined effects of thermal radiation and Hall current on MHD free-convective flow and mass transfer over a stretching sheet with variable viscosity. Retrieved from http://arxiv.org/abs/1008.0165v1
[17] Tamizharasi, P., Vijayaragavan, R., & Magesh, A. (2021). Heat and Mass transfer analysis of the peristaltic driven flow of nanofluid in an asymmetric channel. Partial Differential Equations in Applied Mathematics
[18] Wajihah, S. A., & Sankar, D. S. (2023). A review on non-Newtonian fluid models for multi-layered blood rheology in constricted arteries. Archive of Applied Mechanics, 93(5), 1771-1796
[19] Wu, W. T., & Massoudi, M. (2020). Recent Advances in Mechanics of Non-Newtonian Fluids. Fluids, 5(1), 10
[20] Yang, R., Christov, I. C., Griffiths, I. M., & Ramon, G. Z. (2020). Time-averaged transport in oscillatory squeeze flow of a viscoelastic fluid. Physical Review Fluids, 5(094501)


ISSN 1584 – 2665 (printed version); ISSN 2601 – 2332 (online); ISSN–L 1584 – 2665